J Appl Biotechnol Rep. 2025 December;12(4):1815-1827

Journal of
Applied Biotechnology Reports

doi 10.30491/jabr.2025.558418.1941

Original Article

Facilitating Wound Healing by Inducing M2 Macrophage Polarization Using Polymeric Nanoparticles; an Experimental and Molecular Study

Hamid Kooshki [1†], Mehrdad Rezaeian [2†], Reza Heidari [2,3,4], Mozafar Mohammadi [5], Ali Shakerimoghaddam [6], Sakineh Hajebi [7], Zahra Hami [8], Ali Saberian [9], Mostafa Shahrezaee [10], Mohsen Chamanara [8*]

[1] Nanobiotechnology Research Center, New Health Technologies Institute, Baqiyatallah University of Medical Sciences, Tehran, Iran
[2] Cancer Epidemiology Research Center, AJA University of Medical Sciences, Tehran, Iran
[3] Infectious Diseases Research Center, AJA University of Medical Sciences, Tehran, Iran
[4] Medical Biotechnology Research Center, AJA University of Medical Sciences, Tehran, Iran
[5] Applied Biotechnology Research Center, New Health Technologies Institute, Baqiyatallah University of Medical Sciences, Tehran, Iran
[6] Noncommunicable Diseases Research Center, Neyshabur University of Medical Sciences, Neyshabur, Iran
[7] Biomaterial and Medicinal Chemistry Research Center, AJA University of Medical Sciences, Tehran, Iran
[8] Toxicology Research Center, AJA University of Medical Sciences, Tehran, Iran
[9] Faculty of Agriculture, Shahrekord Branch, Islamic Azad University, Shahrekord, Iran
[10] Trauma Research Center, AJA University of Medical Sciences, Tehran, Iran

Corresponding Author: Mohsen Chamanara, PhD, Professor, Toxicology Research Center, AJA University of Medical Sciences, Tehran, Iran. Tel: +989358644606, E-mail: chamanaramohsen@gmail.com
† These authors contributed equally to this work: Hamid Koshki and Mehrdad Rezaeian.

Received November 9, 2025; **Accepted** November 29, 2025; **Online Published** December 30, 2025

Abstract

Introduction: Targeting macrophages has garnered significant research interest due to their pivotal role in inflammation, cancer, and wound healing. This study investigates the impact of nanoparticle design on macrophage interactions and its subsequent influence on wound healing.

Materials and Methods: Four nanoparticles (hyaluronic acid, chitosan, dextran, and methacrylic acid) were selected based on their biocompatibility and targeting potential. Molecular dynamics simulations revealed that hyaluronic acid exhibited the most favorable interactions with the macrophage membrane, positioning it as a promising candidate. To validate these findings, an *in vivo* experiment was conducted using hyaluronic acid nanoparticles on wounded rabbits.

Results: The results showed that the factors involved in the stability of hyaluronic acid nanoparticles, including contact area average (40 nm^2), Gyration Radius analysis (4.5 nm) and time dependent Rg (5.8 nm) were at their lowest level compared to another nanoparticle. Also the lowest entropy (700 kj/mol.k), minimum distance(1.1 nm) and energy average(-2000 kj/mol) showed the appropriate stability of hyaluronic acid nanoparticles. The results demonstrated that topical administration of hyaluronic acid nanoparticles significantly accelerated wound healing. The formulation had an average hydrodynamic diameter of approximately 104 ± 25 nm, a zeta potential of –18 ± 2 mV, and a polydispersity index (PDI) of 0.306. HA nanoparticles significantly reduced wound size compared to the control group on days 7, 14, and 21 ($p < 0.01$).

Conclusions: This study utilized molecular dynamics simulations (MDS) to explore the interaction between four nanoparticles (hyaluronic acid, chitosan, dextran, and methacrylic acid) and the macrophage membrane, focusing on their potential to stimulate macrophages and influence wound healing.

Keywords: Nanomaterials, Wound Healing, Human Macrophages, Polarization, Hyaluronic Acid

Citation: Kooshki H, Rezaeian M, Heidari R, Mohammadi M, Shakerimoghaddam A, Hajebi S, et al. Facilitating Wound Healing by Inducing M2 Macrophage Polarization Using Polymeric Nanoparticles; an Experimental and Molecular Study. J Appl Biotechnol Rep. 2025;12(4):1815-1827. doi:10.30491/jabr.2025.558418.1941

Introduction

Macrophages, as versatile immune sentinels, play a crucial role in wound healing by orchestrating a cascade of events leading to tissue repair and regeneration.[1-3] These dynamic cells exhibit remarkable plasticity, transitioning between pro-inflammatory M1 and anti-inflammatory M2 phenotypes in response to environmental cues.[4] M1 macrophages, characterized by the production of pro-inflammatory cytokines and reactive oxygen species, are essential for initial wound debridement and defense against pathogens.[5-7] However, prolonged M1 activation can impede healing.[8,9] Conversely, M2 macrophages promote tissue repair by secreting growth factors and cytokines that stimulate angiogenesis, collagen deposition, and re-epithelialization.[10,11] Thus, manipulating macrophage polarization towards the M2 phenotype holds

tremendous promise for accelerating wound closure. Nano particles, due to their unique size and surface properties, have emerged as a promising strategy for modulating macrophage polarization.[12,13] They are extensively utilized in biomedicine, with numerous studies examining their interactions with various tissues and cell types.[14,15] Upon administration, phagocytic systems, particularly macrophages (MPs), recognize and internalize these materials as foreign entities, triggering immune responses that can be therapeutically modulated. Surface modification of metallic implants, such as titanium, has been shown to shift macrophage polarization from pro-inflammatory M1 towards reparative M2 phenotypes, enhancing implant integration and reducing inflammation. Similarly, nanomaterial-based immunotherapies have demonstrated efficacy in tumor suppression by reprogramming tumor-associated macrophages (TAMs); for instance, iron oxide nanoparticles (IONPs) induce M1 polarization and diminish M2-like TAM activity. Despite these promising advances, minimizing adverse host immune reactions remains a key challenge, motivating ongoing research into biocompatible nanomaterials and their immunomodulatory effects on MPs.[16,17] Macrophage polarization can be modulated by several biocompatible polymers, particularly glycosaminoglycans and polysaccharides. Hyaluronic acid (HA), a representative glycosaminoglycan, influences macrophage phenotype through its chemical modifications. Highly sulfated HA within collagen matrices suppresses M1 differentiation and favors M2-like macrophages, as evidenced by elevated IL-10 and CD163 expression.[18,19] Similarly, chitosan has been shown to enhance macrophage-derived growth factors, including TGF-β1 and PDGF, promoting ECM synthesis and angiogenesis, while its N-acetylglucosamine residues mediate receptor-specific macrophage activation.[20,21] Oxidized dextran and lipid-based nanoparticles further reinforce this anti-inflammatory profile by upregulating M2 markers (CD206, IL-10, TGF-β) and downregulating pro-inflammatory genes (CD86, TNF-α, IL-6), confirming their immunomodulatory potential independent of drug loading. These findings suggest that strategically designed nanoparticles can be harnessed to tip the balance towards M2 polarization, thereby promoting wound repair.[22,23]

Despite the growing interest in nanoparticle-mediated modulation of wound healing, a comprehensive understanding of the interaction between specific nanoparticles and macrophages is lacking. This study aims to bridge this gap by employing a two-pronged approach: utilizing GROMACS software to investigate the interaction between various polymeric nanoparticles (hyaluronic acid, chitosan, dextran, and methacrylic acid) and the macrophage cell membrane at a molecular level. By analyzing parameters such as interaction energy, contact area, and electrostatic forces, we aim to identify the nanoparticle that exhibits the most favorable interaction profile with the macrophage membrane, potentially leading to enhanced M2 polarization. Based on the findings from the *in silico* simulations, we will conduct an in vivo experiment to assess the wound healing efficacy of the optimal nanoparticle identified. We will compare wound closure rates and tissue regeneration in a rabbit model treated with the chosen nanoparticle versus a control group. This combined approach, integrating computational modeling with *in vivo* experimentation, will provide valuable insights into the potential of polymeric nano particles for promoting M2 polarization and accelerating wound healing. The successful outcome of this study could pave the way for the development of novel therapeutic strategies for wound management.

Materials and Methods

Analysis of Particle Size (DLS) and Potential Zeta

The hydrodynamic diameter and zeta potential of the Hyaluronic acid nanoparticles were evaluated using a Malvern Zetasizer Nanosystem (Worcestershire, UK). The aqueous suspension containing the Hyaluronic acid nanoparticles was filtered through a 0.22 μm syringe-driven filter unit. The sizes of the dispersed silver nanoparticles were measured employing the dynamic light scattering (DLS) technique, facilitated by a compact scattering spectrometer from the Malvern Zetasizer Nano series.

Molecular Dynamics Simulation

Molecular dynamics (MD) simulations are computational techniques used to study the physical movements of atoms and molecules within a system. They record and analyze interactions over time, providing insights into atomic positions and influencing system properties. MD data is then transformed into macroscopic values using statistical mechanics, making MD and statistical mechanics complementary.

The temporal evolution of systems is analyzed using Newton's second law in MD simulations. By solving this motion equation, the position of each atom in a system of N atoms can be determined, represented by the equation 1.

$$m_i\left(\frac{d^2 r_i}{dt^2}\right) = F_i\,, \quad i = 1, \ldots, N$$

where (mi) represents the mass of an atom and (Fi) denotes the force exerted by other atoms on that atom. By utilizing Newton's laws of motion, a trajectory can be determined that demonstrates the fluctuations in velocity, position, and acceleration of the particles over time. In molecular dynamics simulations, a physical value is estimated by computing the mean of that quantity throughout the simulation's duration, using the obtained trajectory.[24]

Root-Mean-Square Deviation Analysis

The Root-Mean-Square Deviation (RMSD) was calculated using the following equation, which involves the deviation between the positions of a particle (POi(t)) and a reference particle (Por(t)) at time (t), for a total of (n) particles:

$$RMSD = \sqrt{\frac{1}{n}\sum_{i=1}^{n}\left(P_{O_i}(t) - p_0 r(t)\right)^2}$$

Root-Mean-Square Fluctuation Analysis

The Root-mean square fluctuation (RMSF) is used to determine the difference between a particle's position (i) and a reference point. This metric was calculated through the use of equation 3. The equation considers a specified time period (T) and calculates the average deviation by using the reference position of particle i (riref), which is determined as the average position of the same particle over time.

$$RMSF_i = \left[\frac{1}{T}\sum_{t_j=1}^{T}\left|r_i(t_j) - r_i^{r_{ef}}\right|^2\right]^{1/2}$$

The key distinction between RMSD and RMSF lies in the method of averaging. With RMSF, the average is taken across time for each individual particle i, resulting in a single value for each particle. On the other hand, when calculating RMSD, the average is taken over all particles at a specific time, leading to time-specific values.[25,26]

Energy Analysis

The Van Der Waals (VDW) energy is determined using the Lennard-Jones equation, evaluating the intermolecular force between two atoms or molecules. The intermolecular potential is represented by the letter "V". The parameter "σ" represents the point at which the intermolecular potential between the two particles is zero, and it measures the minimum distance at which the non-bonding particles can approach each other. The van der Waals radius is defined as half the distance between the non-bonding particles. Finally, the "r" symbol represents the distance between both particles, which is calculated as the distance from the center of one particle to the center of the other. To improve the accuracy of molecular simulations, mathematical models similar to those used in optimizing the extraction yield of cell-free fetal DNA can be employed to determine the most influential experimental parameters and minimize energy fluctuations across the system.[27]

$$V_{v\,dw} = 9\left[\left(\frac{\sigma}{r}\right)^{12} - \left(\frac{\sigma}{r}\right)^{6}\right]$$

$$U_{\{E\}}(v) = (4\pi)^{-1}\frac{q_i q_j}{r_{ij}^2}$$

The energy generated by electrostatic interactions is governed by Coulomb's Law, as demonstrated by the following equation:

$$F = \frac{kq_1q_2}{r^2} = \frac{q_1q_2}{4\pi\varepsilon_O r^2}$$

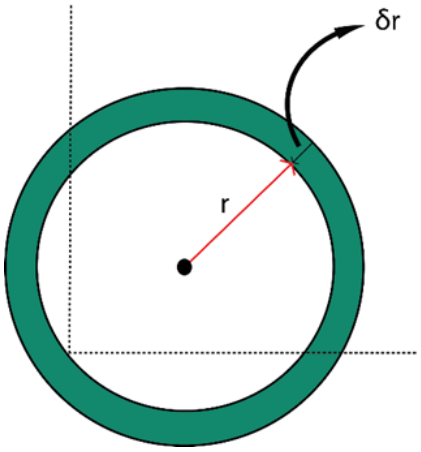

Figure 1. Integral Parameters in Equations to Express Energy Calculations.

The electric force between two charges, q1 and q2, is represented by "F". The distance between the charges is represented by "r". The Coulomb constant is symbolized by "K", while "ε0" represents the permittivity of space.[28]

Gyration Radius

The gyration radius can be obtained using the following formula:

$$R_g = \sqrt{\frac{\sum_{i=1}^{n} r_i^2 m_i}{\sum_{i=1}^{n} m_i}}$$

In this scenario, "n" represents the quantity of particles involved. The mass of particle "i" is represented by "mi", and "r_i" signifies the distance of particle "i" from the center of mass. The parameter "R_g" is used to evaluate the density of the protein during a simulation, and a larger value of R_g indicates a higher density.[29,30]

Radial Distribution Function

The radial distribution function quantifies the likelihood of encountering a pair of atoms at a specific distance "r", compared to the expectation for a completely uniform distribution.

The sampling shell volume:

$$\delta V = \frac{4}{3}\pi(r+\delta r)^3 - \frac{4}{3}\pi r^3 = 4\pi r^2\delta r$$

If a distribution were ideal and homogeneous, the

number of particle pairs present at a specific distance "r" would be contingent on the concentration and the volume of the sampled space.

$$d_{un_i}(r) = \frac{N(N-1)}{V} 4\pi r^2 \delta r$$

The radial distribution function is computed for each individual frame and the resulting values are then taken as the average.[31,32]

Experimental Analysis

Eight fully developed rabbits of both genders were randomly divided into two equal groups. Each group of rabbits was individually housed in cages measuring 45 x 40 x 50 cm. They were all fed the same standard rabbit diet without any restrictions on food or water access. Before the procedure, a designated area on the left thigh of each rabbit was shaved and sterilized with 70% ethanol. Anesthesia was induced by intravenous injection of 20 mg/kg ketamine hydrochloride through the ear vein. Following aseptic surgical techniques, a round incision with an approximate diameter of 1 cm was made through the skin, and the skin was carefully separated from the underlying tissues. 2% Hyaluronic Acid (HA) solution was made by mixing 2 grams of high molecular weight HA powder with 96.9 grams of distilled water and 1.1 grams of Phenoxyethanol-SA (, i.e., 51% Phenoxyethanol, 42% Caprylyl Glycol, and 7% Sorbic Acid). The final solution was applied to the wounds of four rabbits (the study group) twice daily. For the other four rabbits (the control group), a solution of 1.1% Phenoxyethanol-SA in water without HA was applied to the wounds twice daily. The wounds of all 8 rabbits were then covered with two-ply gauze secured by elastic adhesive tape. The hyaluronic acid (HA) nanoparticles used in this study were procured from a commercial supplier (Nanobiotech Co., Tehran, Iran) as a pre-formulated sterile powder designed for biological applications. According to the manufacturer's certificate of analysis, the material consisted of crosslinked HA nano particles prepared via ionic gelation of sodium hyaluronate. The formulation had an average hydrodynamic diameter of approximately 120 ± 25 nm, a zeta potential of –18 ± 2 mV, and a polydispersity index (PDI) of 0.21. The nanoparticles were dispersed in distilled water at a final concentration of 2% (w/v) for topical administration. Although direct DLS and zeta potential measurements were not repeated in our lab due to limited sample availability, these physicochemical specifications are consistent with established parameters for biocompatible HA-based colloids used in previous wound healing and macrophage-modulation studies.[32,33]

The 8 rabbits received sedation on postoperative days 7, 14, and 21, respectively. Pictures of the wounds were taken from an approximate distance of 10 cm using the same camera for all rabbits on mentioned days. The surface area of the wounds was calculated using CorelDraw software in square millimeters and the scales were then changed to percentage of the wound surface area on day 0 for each rabbit wound so probable minor operation and photography mistakes are compensated.

Mean percentage was calculated in the study and control groups separately for days 0, 7, 14, and 21, and two-sample t-test was performed using SPSS software to see if the wound size difference between the two groups are significant on mentioned days ($p \leq 0.01$).

$$t = \frac{\bar{x}_1 - \bar{x}_2}{\sqrt{s^2\left(\frac{1}{n_1} + \frac{1}{n_2}\right)}}$$

$$s^2 = \frac{\sum_{i=1}^{n_1}(x_i - \bar{x}_1)^2 + \sum_{j=1}^{n_2}(x_j - \bar{x}_2)^2}{n_1 + n_2 - 2}$$

Statistical Analysis

The data with the normal distribution involved a one-way analysis of variance (ANOVA). A significance level was set at $p < 0.05$, conducted using SPSS software version 23.

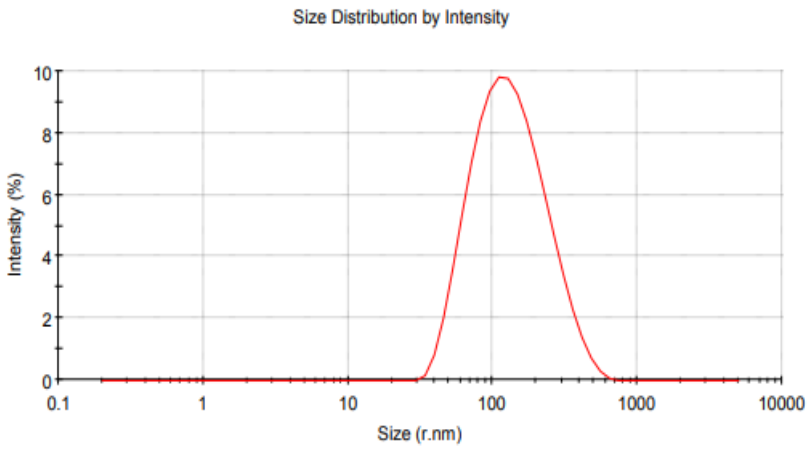

Figure 2. Hyaluronic Acid Nanoparticles Size Distribution by Intensity. The Z Average Equal to 104 nm with PDI:0.306.

Results

Characterization of Hyaluronic Acid Nanoparticles

The results of the tests with the ZetaSizer device on hyaluronic acid nanoparticles showed that the average particle size is approximately 104 nm with a PDI of about 0.306.

Molecular Simulations

Figure 3 displays the representation of the simulation results of the 4 polymers and the macrophage membrane interaction. In this section, we will examine different aspects of the interaction between the nanoparticles and the macrophage membrane, evaluating their efficiency and the response they elicit in the macrophage. After 1000 ns of simulation, the results showed that Hyaluronic acid had the highest degree of integration with the membrane and had completely penetrated it. This outcome is indicative of its favorable properties for simulating macrophage responses.[33,34]

Interaction Distance and Energy Profiles

As shown in Figure 3a–c, the molecular dynamics simulations revealed distinct interaction behaviors between the examined nanoparticles and the macrophage membrane throughout the 1800 ns trajectory. Entropy analysis (Figure 3a) demonstrated a substantial reduction for HA, indicating enhanced molecular ordering and aggregation on the membrane surface; chitosan and dextran showed moderate decreases, while MAA displayed an entropy increase, reflecting weaker membrane association. The average minimum distance (Figure 3b) analysis further confirmed that HA remained consistently closest to the macrophage membrane, signifying stronger adhesion and persistent interaction, whereas MAA maintained the largest separation distance. Correspondingly, the interaction energy profiles (Figure 3c) showed that HA possessed the highest VDW contribution and total interaction energy, followed by chitosan, dextran, and MAA. Although MAA exhibited a relatively high electrostatic component, its overall energy was diminished due to the weak VDW forces and greater interfacial separation. These combined results indicate that the superior affinity and stimulatory capacity of HA toward the macrophage membrane primarily originate from short-range VDW-dominated interactions, leading to a more stable and compact adsorption pattern consistent with its *in-vivo* wound-healing performance described later. Consistent with the MDS profiles, HA showed the smallest mean distance and the strongest total interaction energy with the macrophage membrane. This explains its superior stability and bioactivity observed in the *in vivo* wound-healing model.

Average of Minimum Distance

Figure 3b illustrates the average minimum distance between the selected nanoparticles and the macrophage. Methacrylic acid exhibits a considerable difference from the other three polymers, indicating that it has had minimal interaction and thus resulted in an assessment of interaction energies. The interaction energies between the nanoparticles and the macrophage membrane directly influence the interaction strength and macrophage simulation. Both the bond type and the amount of interaction energy play important roles in molecular interactions. Figure 2c shows the comparison of interaction energies between nanoparticles and macrophage membranes. There were clear patterns in the van der Waals forces (VDW), electrostatic interactions, and overall interaction energy. In particular, Hyaluronic acid had the highest VDW energy, which means that the nanoparticle and membrane are strongly attracted to each other. These forces were gradually lower for chitosan, dextran, and methacrylic acid. Methacrylic acid showed the most favorable electrostatic interactions with the membrane, indicating the potential electrostatic attraction between the negatively charged nanoparticle and the positively charged areas in the macrophage membrane. Hyaluronic acid, chitosan, and dextran were associated with the reduction of electrostatic interaction energies. When considering the combined effects of VDW forces and electrostatic interactions, hyaluronic acid emerged as the clear winner. It had the highest total interaction energy, reflecting a strong overall attraction to the macrophage membrane. On the contrary, methacrylic acid showed the lowest total interaction energy. These findings indicate that hyaluronic acid has the most favorable energy profile for interaction with the macrophage membrane, potentially leading to increased cellular uptake and biological effects. To conclude our evaluation of this factor, it's important to note that VDW forces are significantly more potent than electrostatic forces. Based on our findings, Hyaluronic acid generates the strongest bonds and is the most effective in stimulating macrophages, followed by Chitosan, Dextran, and Methacrylic acid which have weaker immunological responses. The other nanoparticles have a lower average minimum distance, indicating their proximity to the macrophage membrane and their ability to interact and stimulate macrophages more effectively. Ultimately, Hyaluronic acid is the superior option, with Chitosan and Dextran following in that order.[35]

Interaction Energies

The strength of the connection between the nanohybrids and the macrophage membrane is directly related to the level of interaction and the simulation of the macrophage. The type of bond and the amount of energy involved in the interaction are both critical elements that determine molecular interactions. Figure 3c presents a comparison of VDW forces, electrostatic energy, and overall interaction energy for each nanoparticle and the macrophage membrane. The results reveal that hyaluronic acid exhibits the highest VDW energy, followed by chitosan, dextran, and finally

methacrylic acid. In terms of electrostatic forces, methacrylic acid performs the best, followed by hyaluronic acid, chitosan, and dextran. Finally, when assessing total energy, hyaluronic acid ranks first, followed by chitosan, dextran, and methacrylic acid, with hyaluronic acid exhibiting the highest total energy and methacrylic acid the lowest. In summary, it is essential to note that van der Waals (VDW) forces are significantly more robust than electrostatic forces. Nonetheless, in terms of activating and eliciting a response from macrophages, hyaluronic acid forms the strongest bonds and is thus the most effective, followed by chitosan, dextran, and methacrylic acid in descending order.[36,37]

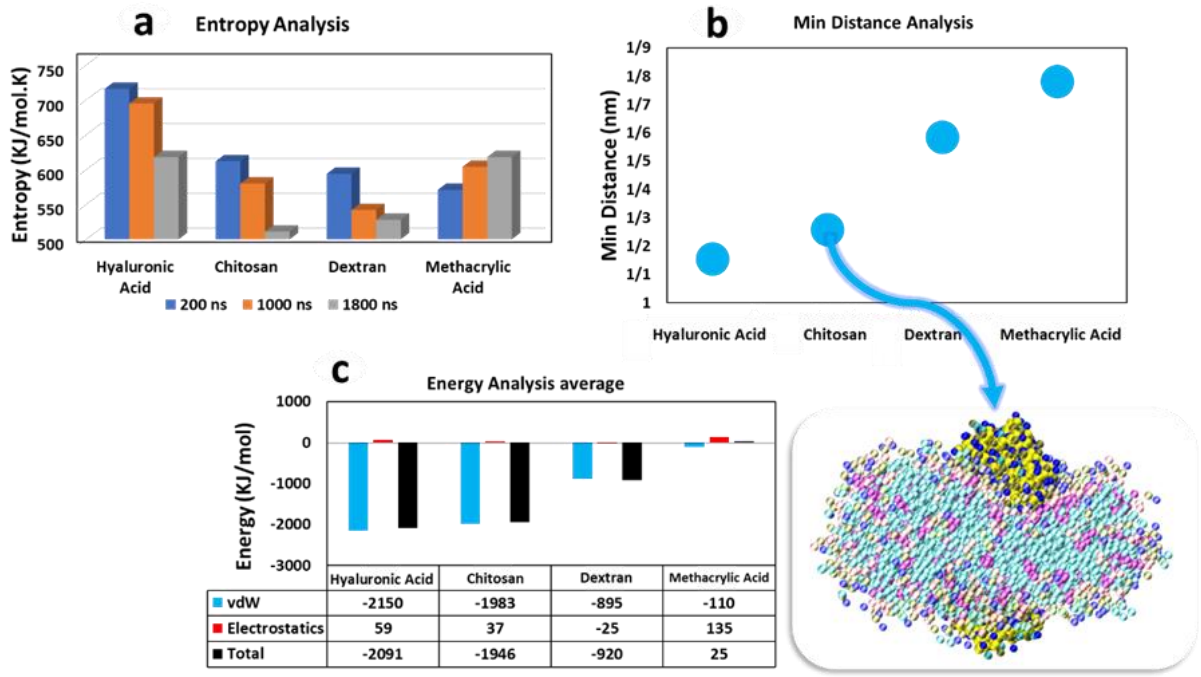

Figure 3. Distinct Interaction Behaviors between the Examined Nanoparticles and the Macrophage Membrane throughout the 1800 ns trajectory. a) Entropy value for each simulation (Hyaluronic acid, Chitosan, Dextran, and Methacrylic acid) in 200 ns, 1000 ns, and 1800 ns. b) Average of Min Distance value for each simulation. c) Average of VDW, Electrostatics, and Total Energies for each simulation.

Average Contact Area

Figure 4a shows the average contact area between nanoparticle molecules. Methacrylic acid has the highest value, indicating that its molecules tend to interact with each other rather than the macrophage membrane. Chitosan and dextran show decreasing values, while hyaluronic acid has the least contact area, suggesting its molecules interact more with the macrophage membrane. Based on this parameter, hyaluronic acid demonstrates the best interaction, while methacrylic acid shows the poorest interaction.

Evaluating the Compactness

The gyration radius (Rg) can determine the compactness of a protein structure. A smaller Rg value indicates a more compact macromolecule. Graphs b and c in Figure 3 display the polymer density relative to their distance from the macrophage. A monodisperse graph is not preferred, as it indicates less accumulation and aggregation with the macrophage membrane. Conversely, peaks on the graph close to the macrophage indicate accumulation and aggregation, which correlate with improved macrophage interaction, stimulation, and response. Based on the values from the three graphs in Figure 4, hyaluronic acid is the most preferred polymer due to its lower final Rg and the largest difference between its initial and final gyration radius values. Chitosan, dextran, and methacrylic acid follow as the next preferred polymers, with methacrylic acid being the least preferred due to its monodisperse graph pattern and high final gyration radius value. These characteristics suggest that methacrylic acid has a low tendency to aggregate or accumulate and does not elicit a strong response from macrophage simulation.

Evaluating the Stability

RMSD

RMSD is the primary measure for assessing the stability of a system during MD simulations. It gauges the fluctuations of the particle in question at various time points throughout the simulation, maintaining a constant reference. The steeper the RMSD curve, the more pronounced the oscillations of the particles, indicating a more unstable system. Figure 4a shows the time-dependent RMSD analysis, and Figure 4b presents the average RMSD. As observed, hyaluronic acid, which has the lowest slope

and average RMSD among the studied nanoparticles, demonstrates the most stable interaction with the macrophage membrane, followed by chitosan, dextran, and methacrylic acid.

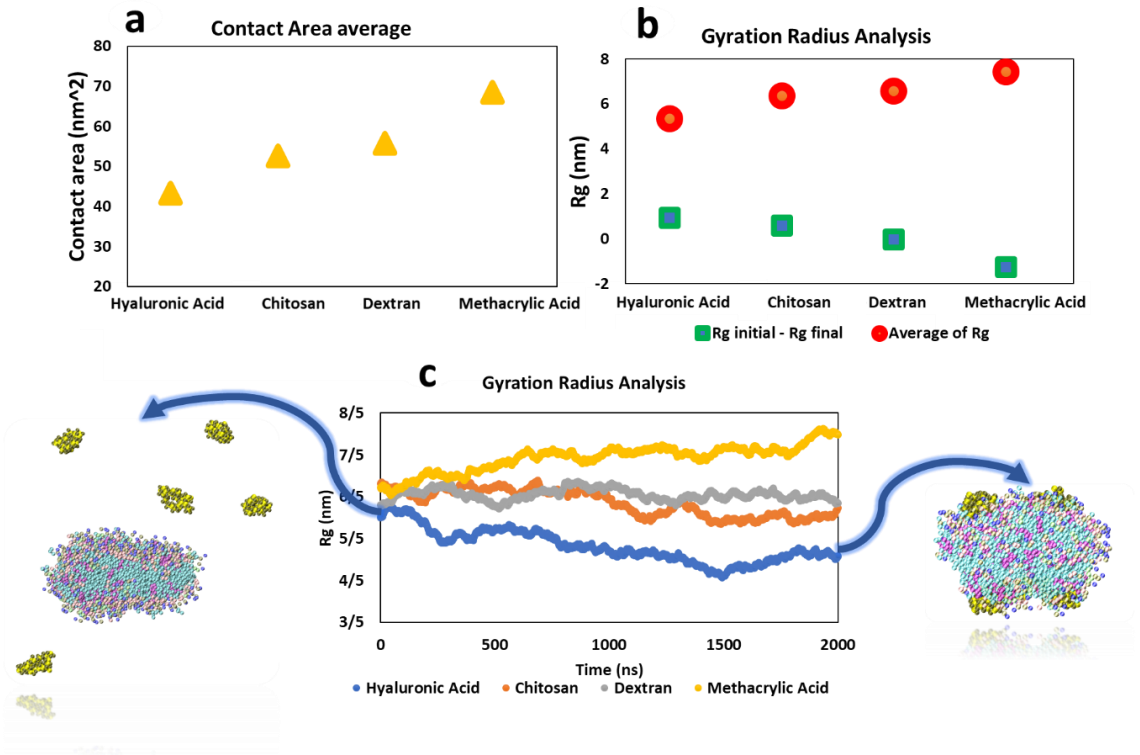

Figure 4. The Parameters Involved in the Stability of Examined Nanoparticles for Each Simulation. a) Average of Contact area analysis for each simulation (Hyaluronic acid, Chitosan, Dextran, and Methacrylic acid). b) The mean and difference of the Rg for the initial and final point of the simulations. c) Time depended Rg.

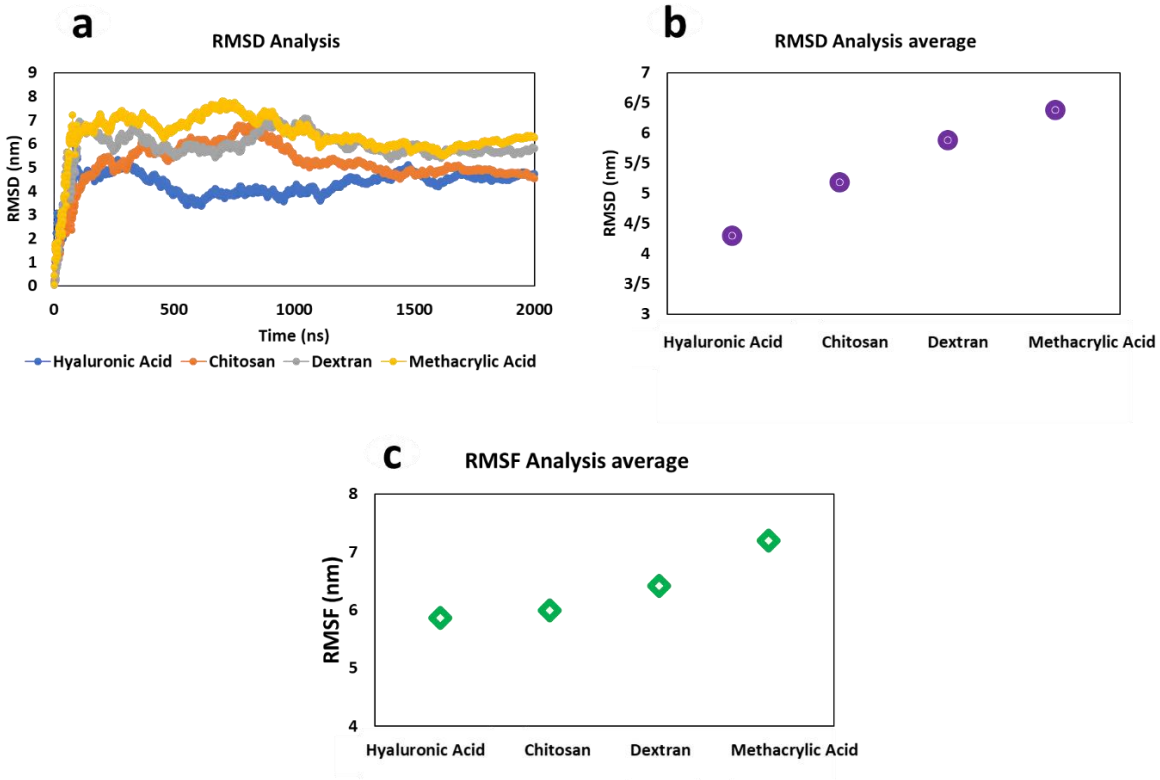

Figure 5. The average of RMSF Values of each Nanoparticle Structure, with Hyaluronic Acid Exhibiting the Most Stability Due to its Lower RMSF Value. a) Time depended RMSD analysis, b) Average of RMSD analysis, and c) Average of RMSF analysis.

RMSF

The RMSF chart displays the fluctuation of each atom during the simulation, with smaller values indicating greater system stability and improved interactions between nanoparticles and the macrophage membrane. Figure 5c compares the average RMSF values of each nanoparticle structure, with hyaluronic acid exhibiting the most stability due to its lower RMSF value, which is associated with membrane stimulation and macrophage signaling. Conversely, methacrylic acid has the highest RMSF value and lowest stability, while chitosan and dextran rank second and third, respectively.

In-vivo Experiments

Eight male New Zealand White rabbits were equally divided into two groups (n = 4/group) including a control group (Rabbits I – IV) without treatment and a study group receiving treatment (Rabbits V – VIII). Full-thickness wounds with a diameter of 1 cm were created on the dorsal region of each rabbit under aseptic conditions. The study group received a topical solution containing 2% hyaluronic acid (HA) twice daily for 21 days. The control group received a

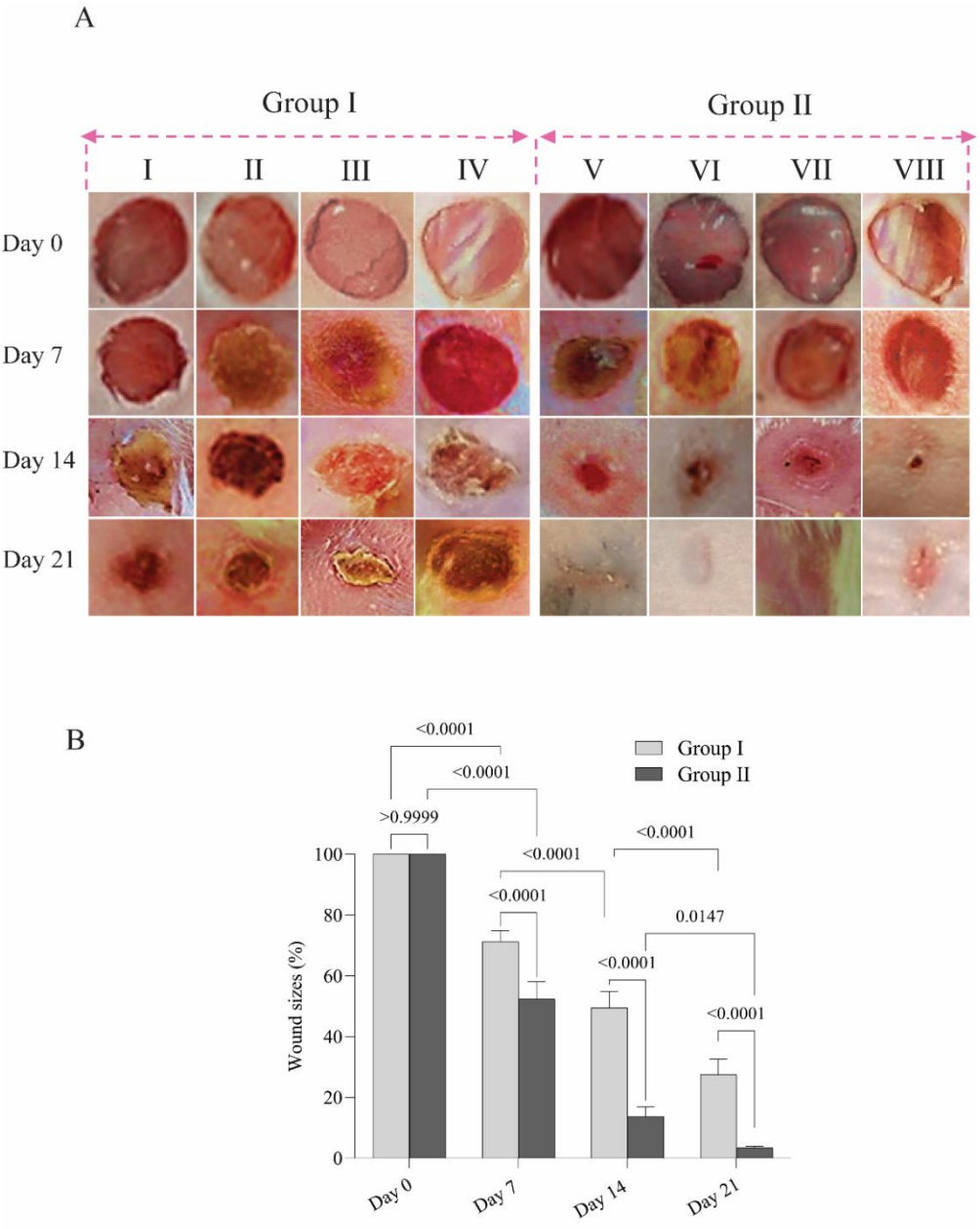

Figure 6. Wound Healing Progression in Rabbit Models Treated with 2% Hyaluronic Acid. (A) Displays representative images of rabbit wounds on days 0, 7, 14, and 21. Rabbits in group I (Rabbits I–IV) served as the control group, while those in group II (Rabbits V–VIII) were treated with 2% hyaluronic acid (HA). Initially (day 0), both groups presented with comparable wound sizes. However, following HA treatment, the study group demonstrated accelerated wound closure, particularly evident by days 7, 14, and 21. (B) Offers a quantitative analysis of the wound size reduction expressed as a percentage of the initial wound area (day 0). Error bars represent the standard deviation derived from n = 4 for each group.

similar solution without HA. To investigate changes in wound size, digital photographs were taken of all wounds on days 0, 7, 14, and 21. Wound surface area was quantified using CorelDraw software and expressed as a percentage of the initial wound size (day 0) for each rabbit. Independent sample t-tests were performed on both the absolute and percentage wound size data to assess the significance of differences between the study and control groups. Images of the wounds revealed a noticeable difference in size between the control and study groups (rabbits I – IV vs. V – VIII). As shown in Figure 6, the initial wound sizes (day 0) were comparable between the two groups ($p < 0.01$). However, following treatment with the 2% hyaluronic acid (HA) solution, wounds in the study group exhibited significantly smaller sizes compared to the control group on days 7, 14, and 21 ($p < 0.01$ for all days). This observation suggests a faster healing process in HA-treated wounds. To account for potential variations in initial wound size, wound surface area was also evaluated as a percentage of the day 0 size for each rabbit (Figure 6). The results of the two-sample t-test performed on this percentage data mirrored those of the absolute wound size data (Figure 6). Wounds in the HA-treated group displayed a significantly greater reduction in wound size compared to the control group on days 7, 14, and 21 ($p < 0.01$ for all days). These findings provide compelling evidence that topical administration of HA significantly accelerates wound healing in rabbits

Discussion

Wound healing is a natural biological process in the human body that progresses through four distinct and well-coordinated stages: hemostasis, inflammation, proliferation, and remodeling.[38] Macrophages play a vital role in this process by exhibiting phagocytic activity and releasing cytokines and growth factors essential for controlling inflammation, fibrosis, and tissue repair. In the initial phase following an injury, M1 macrophages are predominantly active, driving the inflammatory response. As healing advances, the activity shifts to M2 macrophages, which promote tissue regeneration and repair. Enhancing the differentiation and function of M2 macrophages can effectively improve and expedite the wound healing process M2 macrophage polarization describes the differentiation of macrophages into the M2 phenotype after exposure to specific signals. Unlike M1 macrophages, which are pro-inflammatory, M2 macrophages are crucial for anti-inflammatory responses and tissue repair. Key steps involved in M2 macrophage polarization include: (i) stimulation of macrophages using signals such as IL-4, IL-13, glucocorticoids, or polyamines; (ii) activation of intracellular signaling pathways, including STAT6 and PPARγ; (iii) reprogramming macrophage gene expression toward the M2 phenotype; (iv) upregulation of M2-specific markers, such as CD206, CD163, and Arginase-1; and (v) increased production of anti-inflammatory cytokines, such as IL-10 and TGF-β, enhancing macrophage capacity for apoptotic cell clearance and tissue regeneration. Overall, M2 macrophage polarization shifts macrophages to a reparative and anti-inflammatory state, making them pivotal in wound healing and tissue repair.[38,40] A novel strategy for improving wound healing involves utilizing M2 macrophage polarization. Nanoparticles have shown great potential in this area due to their strong antimicrobial properties and low cytotoxicity reported in numerous studies.[41-43] By simultaneously promoting M2 macrophage polarization and providing antibacterial effects, nanoparticles can play a significant role in preventing infections and accelerating the wound healing process.[44,45]

The present study investigated the effect of nanoparticles of hyaluronic acid (HA), dextran, chitosan, and methacrylic acid on M2 macrophage polarization. Initially, Molecular Dynamics Simulation (MDS) was employed to identify the most effective nanoparticles using analyses such as RMSD, RMSF, energy analysis, gyration radius, and radial distribution function. The most effective nanoparticle was then tested on animal models, and the results demonstrated a significant reduction in wound size. Among the tested nanoparticles, hyaluronic acid showed the highest efficacy due to its superior accumulation at the macrophage membrane, closer proximity to the membrane, better binding interactions, higher structural density, and greater stability, as indicated by DMS analyses. These findings were further corroborated in animal experiments, where HA nanoparticles significantly reduced wound size compared to the control group on days 7, 14, and 21 ($p < 0.01$). Similar to our findings, a study by Chu and colleagues[46] demonstrated that TMP-HA-loaded HA hydrogel (Tetramethylpyrazine-loaded HA) significantly accelerated wound healing compared to commercially available INTRASITE gel loaded with TMP. This improvement was evident through reduced inflammation, enhanced angiogenesis, and increased collagen deposition. In that study, macrophage polarization was associated with Tetramethylpyrazine, whereas our findings suggest that hyaluronic acid itself can induce a similar effect. Additionally, a study by Rangasami and colleagues[47] showed that the combination of HA-DEX-DOX (dexamethasone hyaluronic acid-chemotherapeutic agent, doxorubicin) shifted bone marrow-derived M2 macrophages towards the inflammatory M1 phenotype by enhancing cytokines TNF-α, iNOS, and IL-1β. This indicates that HA-based compounds may influence macrophage polarization, although the focus of their study was on antitumor effects. In another study conducted by Zhao et al.,[48] the relationship between ALPK1, hyaluronic acid, and M1 macrophage polarization in temporomandibular joint inflammation was investigated. It was found that hyaluronic acid inhibited M1 macrophage polarization. These findings suggest that HA may not only

promote M2 macrophage polarization but also inhibit M1 polarization, although further research is required to confirm this. Furthermore, a study by Yuan and colleagues[49] demonstrated that extracellular vesicles derived from M2 macrophages, encapsulated in hyaluronic acid, alleviated osteoarthritis by promoting M2 macrophage polarization. This highlights the pivotal role of hyaluronic acid in inducing M2 macrophage polarization. In conclusion, most studies, including ours, indicate that hyaluronic acid induces M2 macrophage polarization and may also inhibit M1 polarization. However, additional studies are warranted to further elucidate these mechanisms in the future. The favorable molecular dynamics parameters observed for HA nanoparticles, namely their higher van der Waals energy, reduced RMSD and RMSF values, and shorter interaction distance with the macrophage membrane, suggest a stable and prolonged membrane association that could influence early signaling events. Such strong and sustained contact may facilitate clustering of membrane receptors such as CD44 and TLR2/4, which are known HA-binding and macrophage-regulatory proteins. This enhanced receptor engagement may in turn activate downstream cascades, including the PI3K-Akt and STAT6 pathways, promoting the transcription of anti-inflammatory cytokines (IL-10, TGF-β1) while suppressing NF-κB-mediated pro-inflammatory signaling. Hence, the physicochemical stability of HA at the bio-nano interface, predicted by MDS, provides a plausible molecular basis for its ability to drive the M1-to-M2 phenotypic transition observed *in vivo*.

Hyaluronic acid not only promotes macrophage polarization but also possesses antibacterial properties that contribute to both wound healing and infection prevention. A study conducted by Guzińska et al.[50] examined the antibacterial activity of highly porous structures made from hyaluronic acid. The findings revealed significant antibacterial effects against both Gram-positive and Gram-negative bacteria. Additionally, various other studies have highlighted the antibacterial efficacy of hyaluronic acid against major wound infection-causing bacteria such as Pseudomonas aeruginosa, Staphylococcus aureus, and others.[51,52] Hyaluronic acid exerts its antibacterial effect by specifically binding to bacterial cell membranes, using them as a target for its activity.[53] This interaction disrupts the structure and function of the bacterial membrane, causing cellular content leakage and ultimately bacterial cell death.[54,55] Moreover, hyaluronic acid can be combined with other antibacterial agents, such as zinc oxide nanoparticles, silver nanoparticles, or plant extracts, to enhance its bactericidal properties. However, further research is needed to evaluate how such combinations might influence macrophage polarization, which is recommended as a direction for future studies. Beyond its direct role in macrophage modulation, the antibacterial activity of hyaluronic acid may further sustain a pro healing microenvironment favorable to M2 polarization. By lowering the bacterial burden and reducing pathogen associated molecular patterns (PAMPs), HA minimizes continuous TLR driven activation of pro inflammatory M1 macrophages. This suppressed bacterial stimulation enables a faster resolution of inflammation and facilitates the shift toward IL 10 and TGF β mediated M2 responses. Consequently, the antibacterial effect of HA can be viewed as a complementary mechanism that indirectly reinforces its immunomodulatory and regenerative roles in wound healing.

Conclusion

This study employed molecular dynamics simulations (MDS) to investigate the interaction between four nano particles (hyaluronic acid, chitosan, dextran, and methacrylic acid) and the macrophage membrane, assessing their potential for stimulating macrophages and influencing wound healing. Various parameters, including interaction energies, entropy, stability, compactness, distance, and contact area, were analyzed. Overall, the molecular dynamics simulations demonstrated that HA possesses the most stable and energetically favorable interaction with the macrophage membrane, characterized by reduced entropy, lower RMSD/RMSF, higher total interaction energy, and greater membrane proximity. This favorable interaction profile likely facilitates enhanced uptake of HA by macrophages and promotes a shift toward the reparative M2 phenotype. The in vivo rabbit wound model confirmed this mechanism, as HA treatment resulted in significantly accelerated wound closure compared with controls. Together, these findings highlight a mechanistic link between HA–membrane interactions and macrophage-mediated wound repair, underscoring HA nanoparticles as a promising immunomodulatory platform for accelerating tissue regeneration.

Authors' Contributions

HK, MM, RH, and MR: Conceptualization, Investigation, Methodology, Data curation, Formal analysis, Writing original draft; MC: Supervision, Validation, Project administration; MR: Conceptualization, Investigation, Methodology, Bibliographic research, Data curation, Formal analysis, Writing-review & editing; AS and MS: Investigation, Bibliographic research, Data curation, Writing-review & editing; ZH and SH: Investigation, Data curation, Formal analysis, Writing-review & editing; SB: Investigation, Data curation, Formal analysis, Writing review & editing.

Conflict of Interest Disclosures

The authors declare that they have no conflicts of interest.

Acknowledgment

We would like to acknowledge the guidance and support

from the "Comprehensive Research Laboratory" of Baqiyatallah University of Medical Sciences. Thanks to guidance and advice from “Clinical Research Development Unit of Baqiyatallah Hospital".

References

1. Pidwill GR, Gibson JF, Cole J, Renshaw SA, Foster SJ. The role of macrophages in *Staphylococcus aureus* infection. Front Immunol. 2021;11:620339. doi:10.3389/fimmu.2020.620339
2. Namdeo P. A review on herbal immunity booster and nutrition–to fight against Covid-19. J Pharm Adv Res. 2021;4(5):1226-37.
3. Sheykhhasan M, Ahmadieh-Yazdi A, Heidari R, Chamanara M, Akbari M, Poondla N, Yet al. Revolutionizing cancer treatment: The power of dendritic cell-based vaccines in immunotherapy. Biomed Pharmacother. 2025;184:117858. doi:10.1016/j.biopha.2025.117858
4. Andrade RG, Reis B, Costas B, Lima SA, Reis S. Modulation of macrophages M1/M2 polarization using carbohydrate-functionalized polymeric nanoparticles. Polymers. 2020;13(1):88. doi:10.3390/polym13010088
5. Yang L, Dai X, Xu Q, Li Y, Liu X, Gao F. Ph-responsive hyperbranched polymer nanoparticles to combat intracellular infection by disrupting bacterial wall and regulating macrophage polarization. Biomacromolecules. 2022;23(10):4370-8. doi:10.1021/acs.biomac.2c00823
6. Akbariqomi M, Kheirandish Zarandi P, Abedi A, Moosazadeh Moghaddam M, Imani Fooladi AA. Bacteria-based immunosuppressive tumor microenvironment reprogramming: a promising dawn in cancer therapy. Microb Cell Fact. 2025;24(1):207. doi:10.1186/s12934-025-02838-2
7. Kooshki H, Abbaszadeh R, Heidari R, Akbariqomi M, Mazloumi M, Shafei S, et al. Developing a DNA aptamer-based approach for biosensing cystatin-c in serum: An alternative to antibody-based methods. Anal Biochem. 2019;584:113386. doi:10.1016/j.ab.2019.113386
8. Singh A, Anang V, Kumari K, Kottarath SK, Verma C. Role of lymphocytes, macrophages and immune receptors in suppression of tumor immunity. Prog Mol Biol Transl Sci. 2023;194:269-310. doi:10.1016/bs.pmbts.2022.10.002
9. Goswami KK, Bose A, Baral R. Macrophages in tumor: An inflammatory perspective. Clin Immunol. 2021;232:108875. doi:10.1016/j.clim.2021.108875
10. Chen S, Saeed AF, Liu Q, Jiang Q, Xu H, Xiao GG, et al. Macrophages in immunoregulation and therapeutics. Signal Transduct Target Ther. 2023;8(1):207. doi:10.1038/s41392-023-01452-1
11. Zhang J, Hu C, Zhang R, Xu J, Zhang Y, Yuan L, et al. The role of macrophages in gastric cancer. Front Immunol. 2023;14:1282176. doi:10.3389/fimmu.2023.1282176
12. Li F, Wang X, Shi J, Wu S, Xing W, He Y. Anti-inflammatory effect of dental pulp stem cells. Front Immunol. 2023;14:1284868. doi:10.3389/fimmu.2023.1284868
13. Zheng H, Cheng X, Jin L, Shan S, Yang J, Zhou J. Recent advances in strategies to target the behavior of macrophages in wound healing. Biomed Pharmacother. 2023;165:115199. doi:10.1016/j.biopha.2023.115199
14. Nikzamir M, Akbarzadeh A, Panahi Y. An overview on nanoparticles used in biomedicine and their cytotoxicity. J Drug Deliv Sci Technol. 2021;61:102316. doi:10.1016/j.jddst.2020.102316
15. Dolai J, Mandal K, Jana NR. Nanoparticle size effects in biomedical applications. ACS Appl Nano Mater. 2021;4(7):6471-96. doi:10.1021/acsanm.1c00987
16. Li Z, Sun L, Zhang Y, Dove AP, O’Reilly RK, Chen G. Shape effect of glyco-nanoparticles on macrophage cellular uptake and immune response. ACS Macro Lett. 2016;5(9):1059-64. doi:10.1021/acsmacrolett.6b00419
17. Cheng J, Zhang Q, Fan S, Zhang A, Liu B, Hong Y, et al. The vacuolization of macrophages induced by large amounts of inorganic nanoparticle uptake to enhance the immune response. Nanoscale. 2019;11(47):22849-59. doi:10.1039/C9NR08261A
18. Qie Y, Yuan H, Von Roemeling CA, Chen Y, Liu X, Shih KD, et al. Surface modification of nanoparticles enables selective evasion of phagocytic clearance by distinct macrophage phenotypes. Sci Rep. 2016;6(1):26269. doi:10.1038/srep26269
19. Cahalane C, Bonezzi J, Shelestak J, Clements R, Boika A, Yun YH, et al. Targeted delivery of anti-inflammatory and imaging agents to microglial cells with polymeric nanoparticles. Mol Pharm. 2020;17(6):1816-26. doi:10.1021/acs.molpharmaceut.9b00489
20. Ibarra LE, Beaugé L, Arias-Ramos N, Rivarola VA, Chesta CA, Lopez-Larrubia P, et al. Trojan horse monocyte-mediated delivery of conjugated polymer nanoparticles for improved photodynamic therapy of glioblastoma. Nanomedicine. 2020;15(17):1687-707. doi:10.2217/nnm-2020-0106
21. He Y, Wang M, Li X, Yu T, Gao X. Targeted MIP-3β plasmid nanoparticles induce dendritic cell maturation and inhibit M2 macrophage polarisation to suppress cancer growth. Biomaterials. 2020;249:120046. doi:10.1016/j.biomaterials.2020.120046
22. Chechushkov AV, Kozhin PM, Zaitseva NS, Lemza AE, Men’shchikova EB, Troitskii AV, et al. Oxidized dextran enhances alternative activation of macrophages in mice of opposite lines. Bulletin of experimental biology and medicine. 2016;160(6):783-6. doi:10.1007/s10517-016-3309-2
23. Harel-Adar T, Mordechai TB, Amsalem Y, Feinberg MS, Leor J, Cohen S. Modulation of cardiac macrophages by phosphatidylserine-presenting liposomes improves infarct repair. Proc Natl Acad Sci U S A. 2011;108(5):1827-32. doi:10.1073/pnas.1015623108
24. Söldner CA, Horn AH, Sticht H. Interaction of glycolipids with the macrophage surface receptor Mincle–a systematic molecular dynamics study. Sci Rep. 2018;8(1):5374. doi:10.1038/s41598-018-23624-8
25. da Fonseca AM, Caluaco BJ, Madureira JM, Cabongo SQ, Gaieta EM, Djata F, et al. Screening of potential inhibitors targeting the main protease structure of SARS-CoV-2 via molecular docking, and approach with molecular dynamics, RMSD, RMSF, H-bond, SASA and MMGBSA. Mol Biotechnol. 2024;66(8):1919-33. doi:10.1007/ s12033-023-00831-x
26. Taidi L, Maurady A, Britel MR. Molecular docking study and molecular dynamic simulation of human cyclooxygenase-2 (COX-2) with selected eutypoids. J Biomol Struct Dyn. 2022;40(3):1189-204. doi:10.1080/07391102.2020.1823884
27. Akbariqomi M, Heidari R, Gargari SS, Omrani MD, Rigi G, Sanikhani NS, et al. Evaluation and statistical optimization of a method for methylated cell-free fetal DNA extraction from maternal plasma. J Assist Reprod Genet. 2019;36(5):1029-38. doi:10.1007/s10815-019-01425-w
28. Philbin JP, Haugland TS, Ghosh TK, Ronca E, Chen M, Narang P, et al. Molecular van der Waals fluids in cavity quantum electrodynamics. J Phys Chem Lett. 2023;14(40):8988-93. doi:10.1021/acs.jpclett.3c01790
29. Maleki R, Afrouzi HH, Hosseini M, Toghraie D, Rostami S. Molecular dynamics simulation of Doxorubicin loading with N-isopropyl acrylamide carbon nanotube in

a drug delivery system. Comput Methods Programs Biomed. 2020;184:105303. doi:10.1016/j.cmpb.2019.105303
30. Miri Jahromi A, Zandi P, Khedri M, Ghasemy E, Maleki R, Tayebi L. Molecular insight into optimizing the N-and P-doped fullerenes for urea removal in wearable artificial kidneys. J Mater Sci: Mater Med. 2021;32(5):49. doi:10.1007/s10856-021-06525-7
31. Haghtalab A, Seyf JY. A new insight to validation of local composition models in binary mixtures using molecular dynamic simulation. AIChE J. 2016;62(1):275-86. doi:10.1002/aic.15038
32. Naeiji P, Varaminian F, Rahmati M. Comparison of the thermodynamic, structural and dynamical properties of methane/water and methane/water/hydrate systems using molecular dynamic simulations. J Nat Gas Sci Eng. 2017;44:122-30. doi:10.1016/j.jngse.2017.04.010
33. Miri-Jahromi A, Didandeh M, Shekarsokhan S. Capability of MXene 2D material as an amoxicillin, ampicillin, and cloxacillin adsorbent in wastewater. J Mol Liq. 2022;351:118545. doi:10.1016/j.molliq.2022.118545
34. Khedri M, Maleki R, Khiavi SG, Ghasemi M, Ghasemy E, Jahromi AM, Razmjou A. Removal of phenazopyridine as a pharmacological contaminant using nanoporous metal/covalent-organic frameworks (MOF/COF) adsorbent. Appl Mater Today. 2021;25:101196. doi:10.1016/j.apmt.2021.101196
35. Khedri M, Afsharchi F, Souderjani AH, Rezvantalab S, Didandeh M, Maleki R, et al. Molecular scale study on the interactions of biocompatible nanoparticles with macrophage membrane and blood proteins. Nano Select. 2022;3(8):1252-63. doi:10.1002/nano.202200043
36. Khedri M, Keshavarz Moraveji M. Biomolecular engineering of drugs loading in Riboflavin-targeted polymeric devices: simulation and experimental. Sci Rep. 2022;12(1):5119. doi:10.1038/s41598-022-09164-2
37. Jahromi AM, Khedri J, Kadir DH, Malekahmadi D, Zandie M, Khedri M, et al. The ability of the absorbed energy in the flat-plate solar-collector'tubes for oil-water separation: an experimental-computational approach. Sustain Energy Technol Assess. 2022;53:102507. doi:10.1016/j.seta.2022.102507
38. Guo SA, DiPietro LA. Factors affecting wound healing. J Dent Res. 2010;89(3):219-29. doi:10.1177/0022034509359125
39. Hassanshahi A, Moradzad M, Ghalamkari S, Fadaei M, Cowin AJ, Hassanshahi M. Macrophage-mediated inflammation in skin wound healing. Cells. 2022;11(19):2953. doi:10.3390/cells11192953
40. Ma Y, Hu J, Xue X, Gu J, Pan Y, Yang J. SENP3 deletion promotes M2 macrophage polarization and accelerates wound healing through smad6/IκB/p65 signaling pathway. Heliyon. 2023;9(5):e15584. doi:10.1016/j.heliyon.2023.e15584
41. Ali W, Jamshidi-Adegani F, Mirsanei Z, Al-Kindi J, Vakilian S, Al-Broumi M, et al. Lanthanide complexes facilitate wound healing by promoting fibroblast viability, migration and M2 macrophage polarization. Dalton Trans. 2024;53(1):65-73. doi:10.1039/D3DT02662K
42. Rahimi M, Piroozmand A, Shayestehpour M, Salamat S, Peik Falak F, Shakerimoghaddam A, et al. Effect of curcumin nanoparticles and alcoholic extract of *Falcaria vulgaris* on the growth rate, biofilm, and gene expression in *Pseudomonas aeruginosa* isolated from burn wound infection. Mol Biol Rep. 2023;50(8):6681-90. doi:10.1007/s11033-023-08559-2
43. Shakerimoghaddam A, Safardoust-Hojaghan H, Amiri O, Salavati-Niasari M, Khorshidi A, Khaledi A. Ca19Zn2 (PO4) 14 Nanoparticles: Synthesis, characterization and its effect on the colonization of *Streptococcus mutans* on tooth surface. J Mol Liq. 2022;350:118507. doi:10.1016/j.molliq.2022.118507
44. Hajebi S, Chamanara M, Nasiri SS, Ghasri M, Mouraki A, Heidari R, et al. Advances in stimuli-responsive gold nanorods for drug-delivery and targeted therapy systems. Biomed Pharmacother. 2024;180:117493. doi:10.1016/j.biopha.2024.117493
45. Li J, Jiang X, Li H, Gelinsky M, Gu Z. Tailoring materials for modulation of macrophage fate. Adv Mater. 2021;33(12):2004172. doi:10.1002/adma.202004172
46. Mao J, Chen L, Cai Z, Qian S, Liu Z, Zhao B, et al. Advanced biomaterials for regulating polarization of macrophages in wound healing. Adv Funct Mater. 2022;32(12):2111003. doi:10.1002/adfm.202111003
47. Chu D, Chen J, Liu X, Liao A, Song X, Li Y, et al. A tetramethylpyrazine-loaded hyaluronic acid-based hydrogel modulates macrophage polarization for promoting wound recovery in diabetic mice. Int J Biol Macromol. 2023;245:125495. doi:10.1016/j.ijbiomac.2023.125495
48. Rangasami VK, Samanta S, Parihar VS, Asawa K, Zhu K, Varghese OP, et al. Harnessing hyaluronic acid-based nanoparticles for combination therapy: A novel approach for suppressing systemic inflammation and to promote antitumor macrophage polarization. Carbohydr Polym. 2021;254:117291. doi:10.1016/j.carbpol.2020.117291
49. Zhao J, Feng Y, Liu X, Li H, Guo H, Ke J, et al. The relationship of ALPK1, hyaluronic acid and M1 macrophage polarization in the temporomandibular joint synovitis. J Cel Mol Med. 2024;28(7):e18172. doi:10.1111/jcmm.18172
50. Yuan Q, Yang M, Zheng H, Cai Y, Luo P, Wang X, et al. M2 macrophage-derived extracellular vesicles encapsulated in hyaluronic acid alleviate osteoarthritis by modulating macrophage polarization. ACS Biomater Sci Eng. 2024;10(5):3355-77. doi:10.1021/acsbiomaterials.3c01833
51. Guzińska K, Kaźmierczak D, Dymel M, Pabjańczyk-Wlazło E, Boguń M. Anti-bacterial materials based on hyaluronic acid: Selection of research methodology and analysis of their anti-bacterial properties. Mater Sci Eng C. 2018;93:800-8. doi:10.1016/j.msec.2018.08.043
52. Federico S, Catania V, Palumbo FS, Fiorica C, Schillaci D, Pitarresi G, et al. Photothermal nanofibrillar membrane based on hyaluronic acid and graphene oxide to treat *Staphylococcus aureus* and *Pseudomonas aeruginosa* infected wounds. Int J Biol Macromol. 2022;214:470-9. doi:10.1016/j.ijbiomac.2022.06.144
53. Del Olmo JA, Alonso JM, Martínez VS, Ruiz-Rubio L, González RP, Vilas-Vilela JL, et al. Biocompatible hyaluronic acid-divinyl sulfone injectable hydrogels for sustained drug release with enhanced antibacterial properties against *Staphylococcus aureus*. Mater Sci Eng C. 2021;125:112102. doi:10.1016/j.msec.2021.112102
54. Zamboni F, Wong CK, Collins MN. Hyaluronic acid association with bacterial, fungal and viral infections: Can hyaluronic acid be used as an antimicrobial polymer for biomedical and pharmaceutical applications?. Bioact Mater. 2022;19:458-73. doi:10.1016/j.bioactmat.2022.04.023
55. Andrade del Olmo J, Pérez-Álvarez L, Sáez Martínez V, Benito Cid S, Pérez González R, Vilas-Vilela JL, et al. Drug delivery from hyaluronic Acid–BDDE injectable hydrogels for antibacterial and anti-inflammatory applications. Gels. 2022;8(4):223. doi:10.3390/gels8040223
56. Qi C, Sun Q, Xiao D, Zhang M, Gao S, Guo B, et al. Tetrahedral framework nucleic acids/hyaluronic acid-

methacrylic anhydride hybrid hydrogel with antimicrobial and anti-inflammatory properties for infected wound healing. Int J Oral Sci. 2024;16(1):30. doi:10.1038/s41368-024-00290-3